MNE 20 (2023) 100218

Contents lists available at ScienceDirect

Micro and Nano Engineering

journal homepage: www.sciencedirect.com/journal/micro-and-nano-engineering

Printed ecoresorbable temperature sensors for environmental monitoring

Nicolas Fumeaux *, Melissa Kossairi, James Bourely, Danick Briand *

École Polytechnique Fédérale de Lausanne (EPFL), Soft Transducers Laboratory (LMTS), 2000 Neuchâtel, Switzerland

ARTICLE INFO

Keywords:
Biodegradable electronics
Temperature sensor
Additive manufacturing
Printing
Zinc
Photonic sintering

ABSTRACT

Electronic waste has become a pressing issue, necessitating sustainable solutions for the disposal of electronic devices. While the development of environmentally degradable electronics has gained attention, the fabrication of stable and performant sensors from biodegradable materials remains challenging. We present printed degradable resistance temperature detectors (RTDs) based on the photonic sintering of a zinc microparticles ink on a cellulosic substrate. Efficient sintering is attained via a two-step process involving electrochemical oxide removal and pulsed light exposure using a xenon lamp. By optimizing the pulse energy and pulse count, we obtain highly linear zinc-based RTDs with a high temperature coefficient of resistance (TCR). The printed zinc reaches a TCR value of 3160 ppm/K, which represents about 80% of the value of the bulk material. The dynamic response of the sensors in a range from −20 to 40 °C closely matches the temperature signal recorded by a commercial sensor. The encapsulation of the screen-printed sensors on paper substrate with a biodegradable beeswax coating ensures protection against the interference of moisture. These printed RTDs, fully made of degradable materials, pave the way to the cost-effective manufacturing of eco-friendly yet performant sensors for environmental monitoring.

1. Introduction

Precise monitoring of ambient temperature is of critical importance for numerous applications in the agriculture, supply-chain, manufacturing, and health care domains [1–4]. Temperature also often needs to be measured for calibration purposes for other types of sensors exhibiting temperature-dependent responses [5–8]. Several sensor designs have been leveraged for various applications and temperature ranges, including negative temperature coefficient (NTC) thermistors, resistance temperature detectors (RTDs), thermocouples or semiconductor-based sensors [9]. RTDs present the advantage to be based on simple resistive devices that can be reliably microfabricated. Their current challenges center around their integration in novel form factors, such as catheters, bioassays, microrobots and wearables [5,10–12]. However, with the increasing number of connected smart objects and sensors in relation to the development of the internet of things (IoT), concerns about electronic waste generation are being raised. As a consequence, more eco-friendly solutions are urgently needed for the manufacturing and disposal of ubiquitous electronic components. Transient electronics, i.e., circuits or devices that can degrade in a specific environment after their desired period of use without generating harmful byproducts, hold promise to address this challenge [13–15]. Due to their increased reactivity and lack of stability when exposed to solvents or high temperatures, the fabrication of microelectronic devices based on degradable materials represents a challenge [16]. Methods to deposit functional layers onto sensitive transient substrates have ranged from the use of a silicone stamp to transfer electronic circuits on the polymeric substrates [17], to shadow-mask deposition techniques to avoid the use of photolithography [18]. These methods have been leveraged to manufacture degradable temperature sensors based on magnesium [19] and silicon nanomembranes [20]. More recently, additive manufacturing methods have emerged as a promising alternative to address this challenge [14]. Printing allows for a more sustainable fabrication process as only the necessary amount of material is deposited, the use of energy-intensive clean room infrastructure and processes is limited or avoided, and scaling up over large area is possible [14,21]. Printing techniques have been leveraged for the production of transient temperature sensors, predominantly based on carbon materials [22–24]. However, metal-based RTDs are well established and present advantages (high stability, conductivity and temperature coefficient of resistance (TCR) [25]), yet the additive fabrication of fully degradable metal-based sensors remains challenging. In recent years, there has been a focus on developing annealing methods for printed transient metals that are compatible with degradable

* Corresponding authors.
E-mail addresses: nicolas.fumeaux@epfl.ch (N. Fumeaux), danick.briand@epfl.ch (D. Briand).

https://doi.org/10.1016/j.mne.2023.100218
Received 14 December 2022; Received in revised form 25 May 2023; Accepted 24 June 2023
Available online 26 June 2023

substrates, which require low process temperatures [26–29]. These efforts have centered around zinc, owing to its wide availability in micro- and nanoparticles form and its lower melting temperature among transient metals [27]. However, a printed degradable metallic layer that can serve as resistive temperature sensor for environmental monitoring or biomedical applications has yet to be demonstrated.

In this work, we present for the first time the additive manufacturing and characterization of a biodegradable zinc temperature sensor. We study the temperature behavior of zinc metallic films printed on paper substrates for the development of RTDs made fully of biodegradable materials. Paper is a cellulose-based material that is recyclable and made of renewable materials [30] and is known to be biodegradable, although the exact biodegradation properties will depend on the paper composition, the treatment method for the cellulose fibers and the environmental conditions during degradation [31,32]. Zinc is an ecoresorbable metal [33,34] and dissolves to zinc oxide and zinc hydroxide in the presence of water [35]. The most commonly used sintering process for printed zinc relies on the electrochemical interaction between zinc oxide and acetic acid, which converts the oxide to zinc metal ions [26]. We combine this method with a photonic sintering process, flash lamp annealing, which consists of delivering high-intensity pulsed light to the printed metal lines [36–38]. This allows to selectively heat the printed patterns with minimal effect on the integrity of the cellulosic substrate. We study the influence of the sintering process on the electro-thermal characteristics of the sensors. The application of the optimum parameters enables printed, transient metallic RTDs with a high linearity and TCR. The effect of ambient relative humidity on the response of the sensors is assessed, and an effective passivation against moisture is achieved with a beeswax coating. Beeswax is chosen here for its water-barrier properties and for its biodegradability, which have been thoroughly investigated, notably in soil [34,39]. The encapsulated sensors are characterized at different ambient humidity levels for temperatures up to 40 °C, demonstrating their usability as fully degradable eco-friendly environmental sensors.

2. Material and methods

2.1. Fabrication

The manufactured zinc RTD on paper substrate is presented in Fig. 1 (d). It consists of a 9.75 mm × 15 mm serpentine resistor with a thickness ranging from 15 to 20 µm and a line width of 250 µm. The resistor was printed from an ink based on Zn microparticles (2 µm average diameter, Sigma Aldrich), polyvinylpyrrolidone (PVP 360 k, Sigma Aldrich) as a binder and 1-pentanol (Sigma Aldrich) as the solvent. The ink was deposited on the paper substrate (Powercoat XD 200 µm, ArjoWiggins) by screen printing through a steel mesh (Serilith) using a silicone squeegee and left to dry for one hour (Fig. 1(a)). After drying, a 10 vol% acetic acid was applied to the metal traces (Fig. 1(b)) by spray coating or drop casting, thereby reducing the native zinc oxide layer, whose high melting point impedes an efficient sintering [26]. After drying of the acetic acid solution on a hotplate for 5 min at 60 °C, the samples were placed in a chamber with a glass sapphire window which was purged with nitrogen. Then, to achieve the sintering of the zinc particles [40], a 30-millisecond photonic flash (Novacentrix Pulseforge 1200) was applied, with pulse energies ranging from 5.1 to 7.3 J/cm^2 (corresponding to lamp voltages between 230 and 260 V), the flash exposure being conducted between one and three times (Fig. 1(c)). Higher pulse energies/number of pulses combinations were not considered as they caused destruction and interruption of the metallic lines. When several energy pulses were used, they were delivered at a frequency of 0.1 Hz, defined to preserve the sample from overheating. This way, the same pulse energy can be delivered several times over, reaching for each light pulse approximatively the same maximal temperature in the metallic layer. For samples that were encapsulated, beeswax (Sigma-Aldrich) was melted in a water bain-marie at approximately 80 °C and the samples were dip-coated and left to dry.

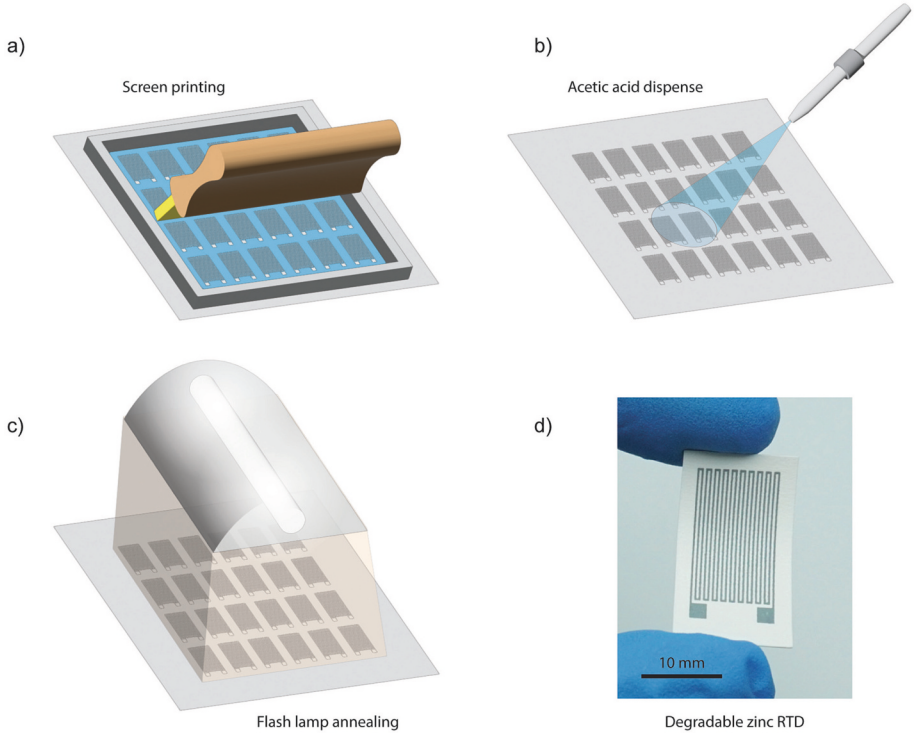

Fig. 1. Fabrication process of the biodegradable RTD. a) Screen printing of the metallic ink. b) Acetic acid spray dispensing on the printed sensors. c) Photonic sintering step. d) Final sensor after cutting out the paper substrate.

2.2. Samples characterization

In order to characterize the electro-thermal behavior of the RTDs, they were placed on a hotplate with a reference temperature and humidity sensor (Sensirion, Digital Humidity and Temperature Sensor, Model SHT4x, operating range: 0–100 %rH, -40-125 °C, relative humidity accuracy: up to ±1.5 %rH, temperature accuracy: up to ±0.1 °C, temperature response time: 2 s) and were covered (**Fig. S1(a)**). The resistance of the samples was acquired with a tabletop multimeter (Keysight Digital Multimeter 34401A) and the temperature was set to a specific setpoint (40 °C, 60 °C or 80 °C) until stabilization. After up to 10 min, the temperature reached a plateau and the hot plate was turned off, with the samples being left to cool to room temperature. In order to disregard different transient thermal behaviors between the reference sensor and the degradable samples, three steady-state resistance values and the corresponding reference temperatures were extracted from the recorded data: the initial room temperature values, the values at the setpoint temperature, and finally values at room temperature after cooling down (**Fig. S1(b)**). The behavior of a resistive temperature sensor with a linear behavior is described by the following equation:

$$R(T) = R_0(1 + \alpha(T - T_0))$$

From the values listed above, the temperature coefficient of resistance (TCR) α of the sintered zinc samples and its degree of linearity (in the form of a squared coefficient of correlation) were determined. Further characterization of the samples was conducted in a climatic chamber (Espec Bench-Top Type Temperature & Humidity Chamber SH-661), in which humidity and temperature can be controlled, and the resistance value was recorded with a data acquisition system (Keysight Data Acquisition/Data Logger Switch Unit 34970A). The humidity was varied between 30 and 70 %rH in steps of three hours and the temperature between 20 and 40 °C in steps of one hour. For cooling experiments from room temperature to 0 °C and 20 °C, the samples were placed with the aforementioned reference temperature sensor between ice packs and in a Liebherr FreezeSafe 8260 freezer, respectively.

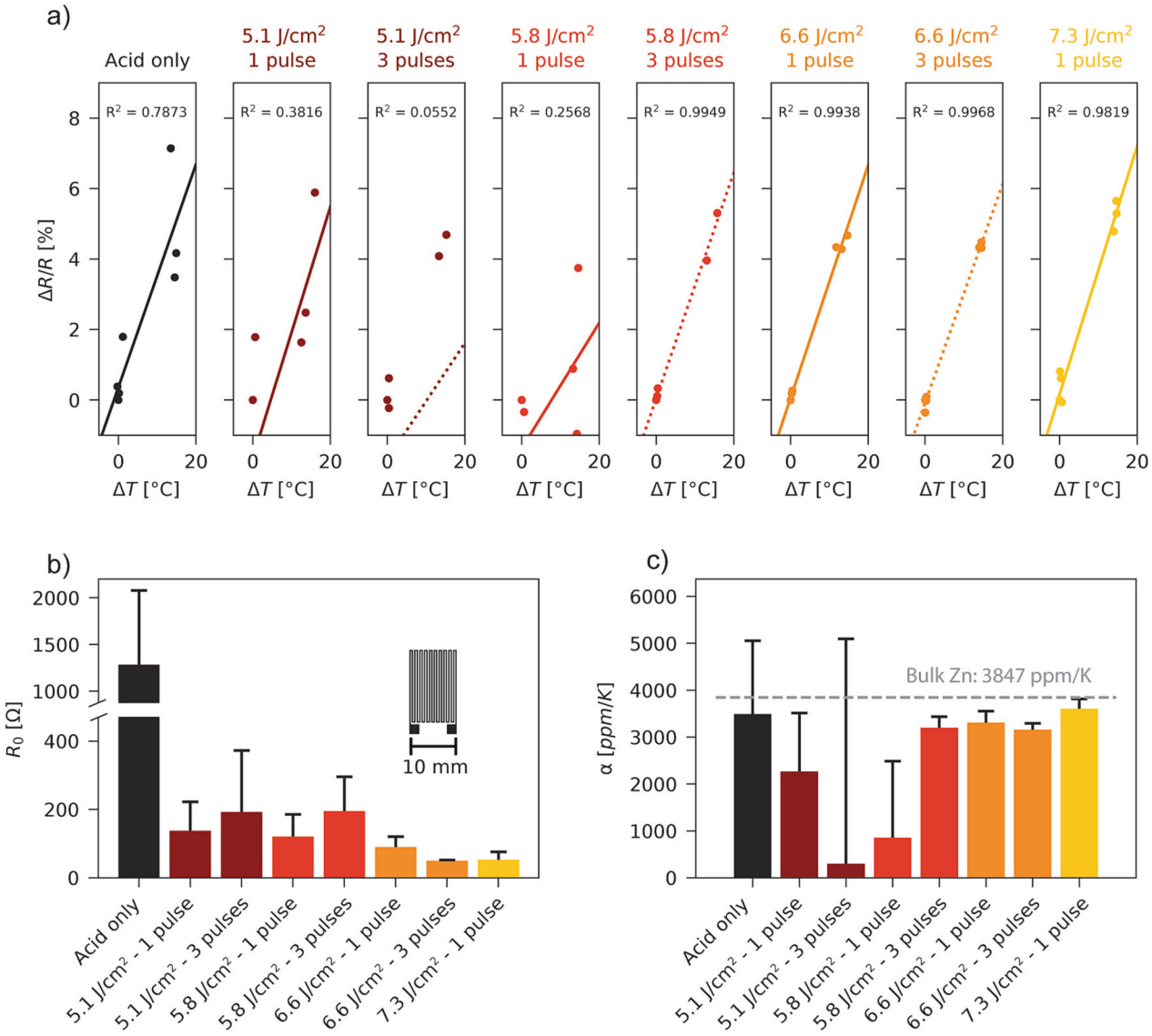

Fig. 2. Influence of the flash energy and number of pulses on the linearity and repeatability of the temperature response of zinc resistors ($n = 3$). a) Relative change in resistance with respect to change in temperature for different sintering parameters. b) TCR as a function of sintering parameters. c) Room temperature resistance as a function of sintering parameters.

3. Results and discussion

3.1. Influence of flash annealing parameters on temperature behavior

The flash lamp annealing approach was investigated and optimized to obtain printed transient zinc metal traces with electro-thermal properties that are applicable to temperature sensing. Fig. 2 shows the influence of the flash lamp parameters (flash photonic energy and number of pulses) on the temperature behavior of the metallic sensing layer. The relative change in resistance is reported with respect to the change in temperature in Fig. 2(a), this for different photonic treatments ranging from no photonic pulses applied (on the left) to increasing pulse energy (5.1 J/cm^2 to 7.3 J/cm^2) and number of pulses (to the right). For each sintering treatment, a squared correlation coefficient (r^2) is shown. The temperature response of a zinc sensor that was sintered only electrochemically (no photonic sintering) is shown in Fig. 2(a), on the left. As can be observed, when only electrochemical sintering is used, the RTDs response exhibits a non-linear behavior and a change of baseline resistance. Different competing effects taking place in the zinc layer can potentially explain this unstable behavior and irreversible changes in electrical conductivity. On one hand, raising the temperature of the sensor accelerates re-oxidation of the Zn particles, which may convert the bridges formed between the particles [41] to zinc oxide and reduce conductivity. On the other hand, heating up the resistor during testing may favor evaporation of acetic acid or water residues in the highly porous layer [26], in this case causing an permanent increase in conductivity. Finally, the presence of polymeric binder in the layer may lead to unstable temperature behavior, as it is known that the purity of the metal layer is paramount for a linear sensing behavior [25]. This can be seen in scanning electron microscope images of the samples, where binder and/or acid residues can be observed around the zinc microparticles after the acetic acid treatment (**Fig. S2**, on the left).

Flash lamp annealing was therefore applied to achieve sintering of the zinc film and stabilize its electro-thermal response. If sufficient energy is delivered during the photonic treatment (as determined by the combination of pulse intensity and number of pulses), the temperature response drastically changes to a linear behavior with minimal hysteresis, as can be seen in Fig. 2(a), on the right. When applying a single pulse, at lower pulse energies (below 5.8 J/cm^2) the temperature response of the zinc layer remains similar to what was obtained with electrochemical sintering only, indicating that the sintering remains incomplete. For one pulse applied, there is a threshold point between 5.8 and 6.6 J/ cm^2 where the temperature response of the sensor becomes highly linear. At the lower pulse energy of 5.8 J/cm^2, processing the samples with three light pulses results as well in a linear temperature response with the squared correlation coefficient r^2 increasing from 0.2568 to 0.9949. Applying three pulses for a pulse intensity of 6.6 J/ cm^2 only slightly improved the linearity of the response to temperature compared to the use of a single photonic pulse for which the linearity was already high. However, applying three pulses at 7.3 J/cm^2 caused excessive damage to the zinc layer, resulting in broken resistors. In summary, a drastic shift in the electro-thermal behavior of the zinc films in terms of linearity is observed when sufficient energy is delivered by the flash annealing treatment, suggesting that the microstructure of the films has been stabilized, as could be expected from literature [42]. The change in electro-thermal behavior when delivering more energy during flash lamp annealing can be explained by the metallic layer reaching a temperature high enough to cause sintering and densification of the particles film [27]. As a consequence of the increased cohesion between the particles, the porosity of the film is reduced and the influence of the corrosion in ambient air becomes less important, resulting in more stable RTDs, whereas, in insufficiently sintered films, the limited bridges between particles may be rapidly oxidized with increasing temperatures. Moreover, the elevated temperatures during photonic sintering can cause decomposition of the organic binder, leading to a more homogeneous metallic layer [43,44] with less impurities, which is associated with a higher temperature dependance of the resistivity [45]. This can also be seen in the SEM images of the zinc layer (**Fig. S2**), where a treatment of three pulses of 6.6 J/cm^2 causes particle fusion and growth and removal of polymeric residue. In parallel, this particles growth results in a decrease of the grain boundary density in the film [46], which can reduce scattering effects and improve temperature sensitivity [47,48]. In summary, the influence of the photonic sintering energy delivered on the temperature response of the printed zinc resistors is thought to be multifactorial, where more effective sintering can lead to increased particle cohesion, reduced grain boundaries and higher homogeneity of the film, contributing to the higher TCR value and the more stable behavior observed.

The sensitivity of the temperature detector scales with the temperature coefficient of resistance of the metal, but also with the initial resistance of the RTD. Increasing the sintering energy causes a decrease in electrical resistivity by one to two orders of magnitude, which translates in an average resistance value going from 1283 Ω for electrochemical sintering alone, down to 48.3 Ω when the highest total energy is delivered (3 light pulses of 6.6 J/cm^2) as seen in Fig. 2(b). On the other hand, the benefit and necessity of using higher energy for the sintering on the RTDs characteristics is clearly seen with an increase in the TCR value, and the linearity and reproducibility of their response. This can be visualized in Fig. 2(a) as well as in Fig. 2(c) which display the average and standard deviation of the TCR of the individual sensors. We see that increasing the sintering energy results in high TCR values for the zinc tracks and that the variability between sensors decreases, making the zinc resistors applicable for stable temperature measurements. Among the set of parameters tested, the TCR reaches a maximal value of 3630 ± 220 ppm/K for one pulse of 7.3 J/cm^2, very close to the one of bulk zinc at 3850 ppm/K [49], while 6.6 J/cm^2, with 1 and 3 pulses, led to a slightly inferior TCR of respectively 3380 and 3050 ppm/K.

Further characterization experiments were conducted on zinc samples exposed to the flash parameter combinations yielding the best electro-thermal characteristics: 1 pulse and 3 pulses at 6.6 J/cm^2, and 1 pulse at 7.3 J/cm^2. When tested up to a temperature of 60 °C, the RTDs that were treated with three pulses of light of 6.6 J/cm^2 show a slightly more reproducible and reversible behavior between samples (**Fig. S3**). The stability of the devices was further assessed by cycling the temperature five times, starting from room temperature and going up to a setpoint of 60 °C to, finally, let them cool down to room temperature again. The sensors that were sintered with three repeated pulses show a more repeatable signal and suffer little baseline drift (Fig. 3(a)). The highest pulse energy applied (7.3 J/cm^2) yields the worst behavior in terms of baseline stability, consistent with the aforementioned hypothesis that some damage is caused to the metallic layer. The use of a multipulse treatment appears to enhance sintering while avoiding excessive damage to the zinc layer. In conclusion, the use of three pulses with an intensity of 6.6 J/cm^2 was deemed to be optimal for the fabrication by printing of degradable Zn RTDs on paper. As a caveat, the optimum flash lamp annealing conditions will vary depending on the layout and thickness of zinc pattern to be sintered and the substrate used, as all of these parameters will impact the temperature distribution across the metallic layer during sintering and therefore the optimal light pulse parameters [38].

As a demonstration, temperature sensors are manufactured with these optimized parameters (i.e., 3 pulses of 6.6 J/cm^2) and their response to temperature are shown in Fig. 3**(b-d)**. The response of the sensor is highly linear as a function of temperature with a TCR value of 3160 ± 130 ppm/K is obtained (Fig. 3(b)), over a range of temperatures from −20 °C to 40 °C. The dynamic measurements conducted at temperatures found in the context of refrigeration and congelation, at 0 °C and -20 °C respectively, can be found in Fig. S4, as this is relevant for application related to supply-chain monitoring. The sensors are able to precisely track variations in temperature and display low hysteresis, as can be seen in Fig. 3(c) as well. The time dynamics of the step response of the sensors are also comparable to commercial sensors (Fig. 3(d)).

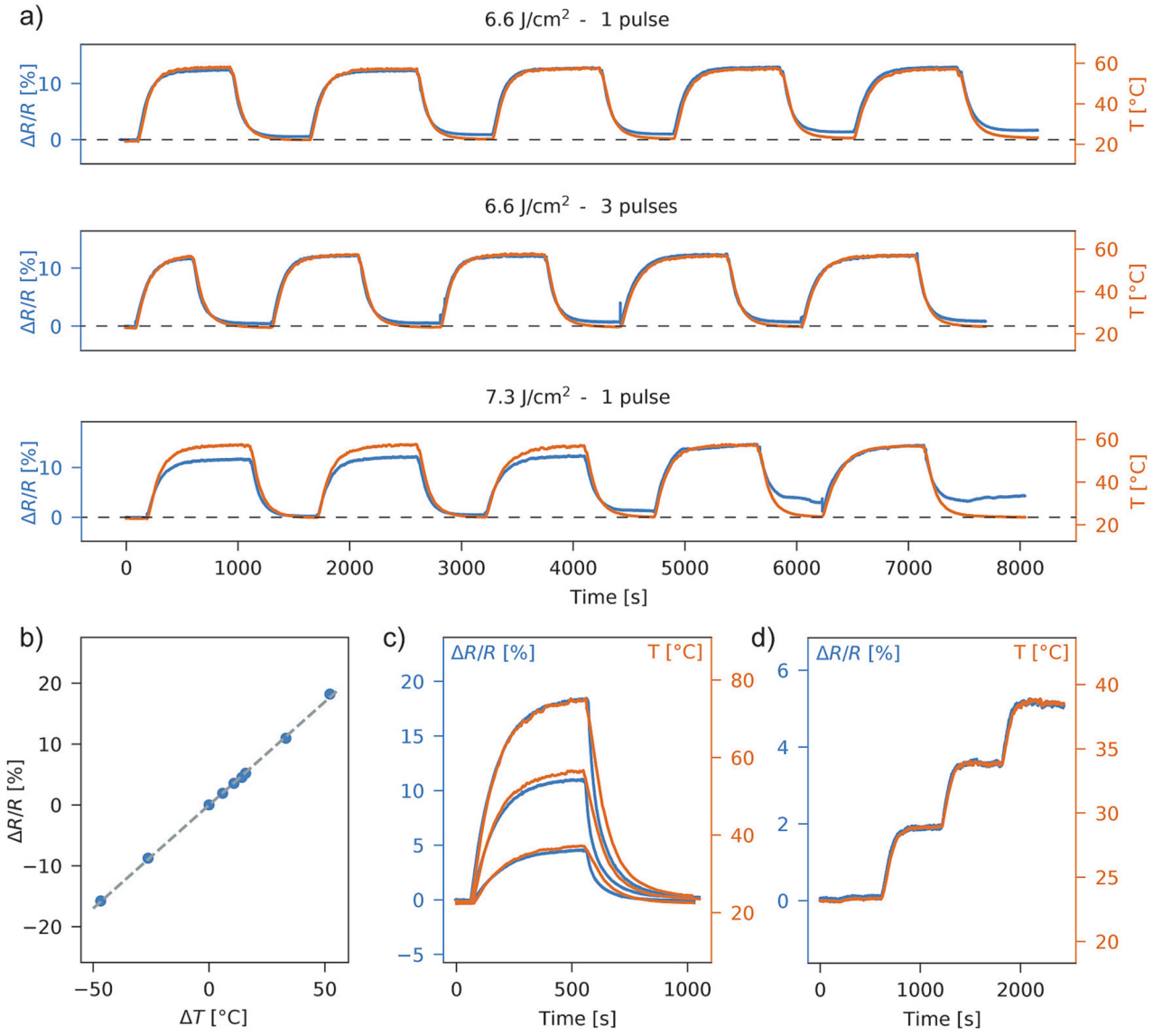

Fig. 3. a) Change in resistance of the zinc traces under cycling between room temperature and 60 °C for three different photonic sintering sets of parameters. b) RTDs calibration curve after sintering with optimal parameters. c) Sensor response (blue) and reference temperature (orange) for different variations in temperature. d) Staircase response of the sensor (blue) compared to a commercial sensor (orange). (For interpretation of the references to colour in this figure legend, the reader is referred to the web version of this article.)

3.2. Influence of ambient humidity on the temperature sensors

A common issue with the use of degradable materials such as zinc for electronics is their sensitivity to water [16,29], which may reduce their performance and stability as sensors. To investigate the influence of ambient humidity on the sintered metallic layer, we first fabricated zinc resistors on a 125 µm polyimide film (PI), which shows limited water absorption. The resistance values for these zinc tracks printed and sintered on PI shows a relative change of between 2 and 5% when humidity is varied between 30 and 70 %rH, as shown in **Fig. S5**. When measuring the resistance of zinc tracks on paper, while varying the ambient humidity between 30 and 70 %rH at a constant temperature of 20 °C, variations in resistance of up to 15% are registered. This results from the water interaction both in the zinc metallic layer and the paper substrate, which may swell and generate a mechanical load in the zinc layer. For both types of substrates, the changes in resistance are maintained after the humidity level has been lowered back to 30 %rH, which may be due to water remaining in the porous layers or partial degradation of the conductive layer in a humid environment, or microcracks having formed in the metallic layer. The relative change in resistance is greater when the zinc layers are printed on a paper substrate, which suggests that stable sensors can only be reached by fully encapsulating them against humidity. It can also be noted that the influence of the ambient humidity is more important at a higher temperature (as seen in **Fig. S4**, on the right), due to the higher absolute humidity content.

We chose to passivate the temperature sensors with beeswax, which, while being a biodegradable and eco-friendly material [50], demonstrates excellent water-barrier properties. Beeswax is already used in food-safe coatings for the preservation of fruit [51–53] and can be applied by dip-coating after heating above its melting temperature of 61–65 °C. To confirm the barrier properties of the coating, the passivated sensors were subjected to the same ambient humidity cycle, as shown in Fig. 4(b). The RTDs display little to no sensitivity to humidity, with an average relative change of resistance of 0.47% after cycling the humidity between 30 and 70 %rH. The behavior of the encapsulated zinc sensors on paper was further tested at temperatures up to 40 °C while maintaining a constant relative humidity, the results being shown in Fig. 5. The sensors respond similarly to the temperature changes,

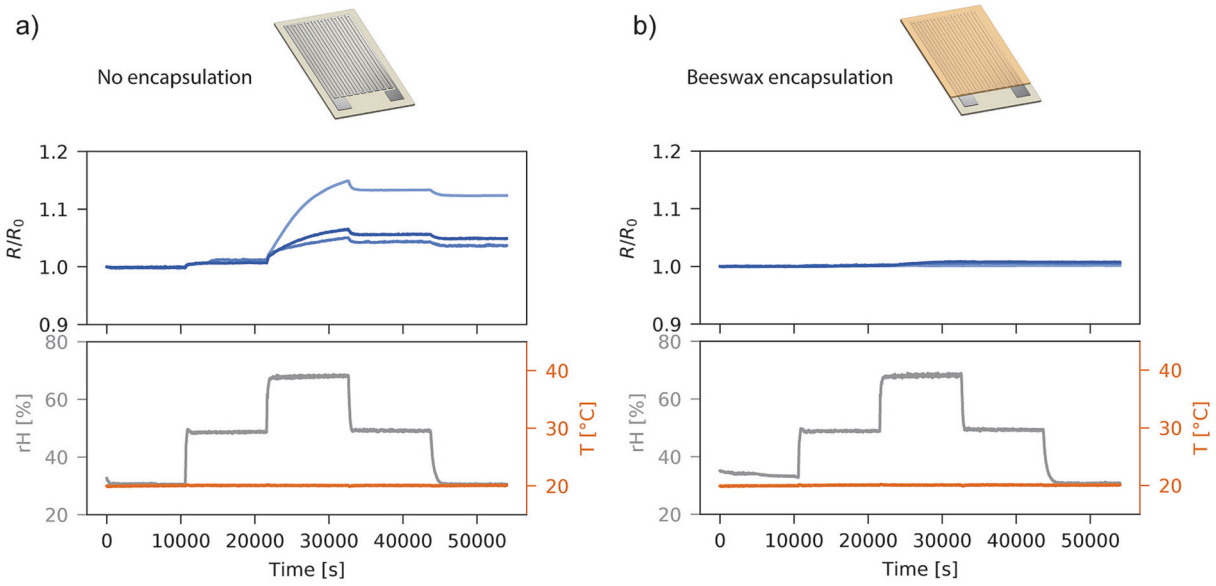

Fig. 4. Relative change of resistance (top graphs) when varying ambient humidity while keeping the temperature at 20 °C (bottom graphs), in the case where: a) the sensors are not encapsulated and b) the sensors are encapsulated with beeswax ($n = 3$).

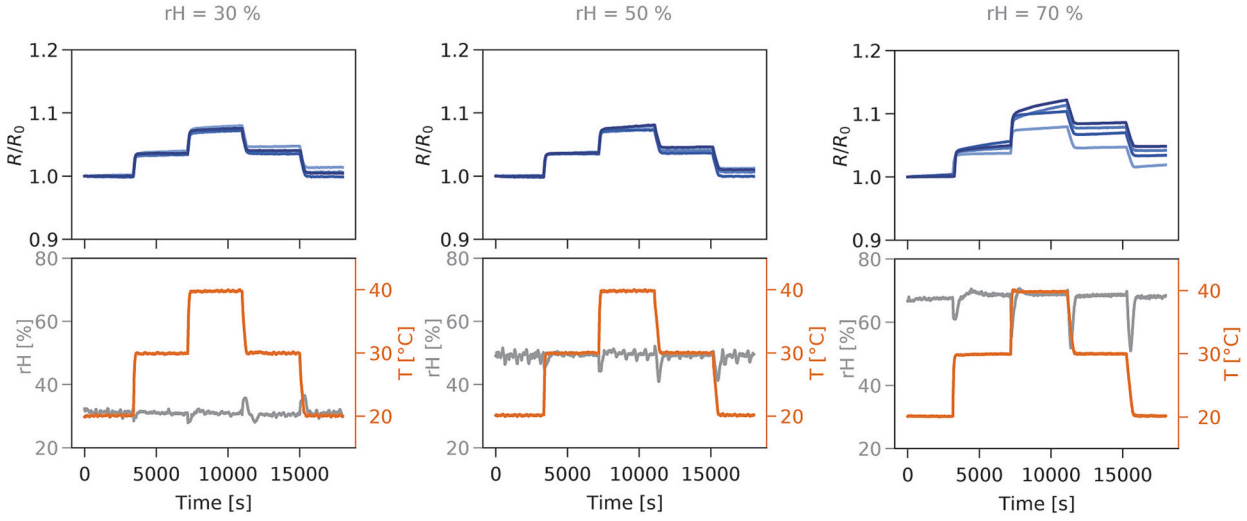

Fig. 5. Relative change of resistance (top) under varying temperature (bottom) for beeswax-encapsulated sensors at various relative humidity levels: 30 %rH (left), 50 %rH (middle) and 70 %rH (right) ($n = 4$).

mostly independently of the humidity level, and the exhibited temperature sensitivity corresponds to the TCR that was previously determined without encapsulation. This result highlights the applicability of the manufactured degradable sensors for supply chain monitoring or digital agriculture purposes. One should notice that some drift is observed at the highest humidity level, especially when the temperature approaches 40 °C. This evidences that improvements on the temperature resilience of the beeswax coating is required to push the operating temperature limits of the sensors.

4. Conclusions

In this work, we show the fabrication and characterization of the first fully printed temperature resistance detector made of degradable metal. The sensors exhibit a linear behavior, with a temperature coefficient of resistance that reaches 80% of that of bulk zinc, and low hysteresis. To this end, a flash lamp annealing process was leveraged and the influence of the photonic pulse energy as well as the number of pulses delivered on the RTDs electro-thermal characteristics was investigated. For this specific layer stack configuration, it was demonstrated that zinc RTDs exhibited a linear temperature response ($r^2 > 0.99$) when subjected to higher pulse energies and pulse counts above the intensity threshold of 5.8 J/cm^2. This outcome is likely attributed to a modification of the microstructure of the zinc layer, allowing to minimize the effect of reoxidation in air and corrosion by water vapor, as well as increased crystallinity and purity of the film after the sintering process. Sensors fabricated with optimized process parameters (3 pulses at 6.6 J/cm^2) were successfully operated at temperatures ranging from −20 °C to 40 °C, exhibiting a dynamic response which is comparable to that of a commercial sensor. Finally, the implementation of a beeswax coating as encapsulation enabled a reliable operation of the RTD sensor under varying ambient humidity levels, with an unaffected response in the range of 30% to 70 %rH. The sensors, made entirely from biodegradable materials, were shown to function within a temperature range compatible with supply chain monitoring, smart farming and generally applications that may require monitoring of the ambient temperature for

a limited period of time. Further developments may include the integration of these RTDs in a fully wireless and biodegradable sensor tag. Finally, this process for zinc could be implemented in the additive fabrication of bioresorbable electronics embedding temperature sensors, systems that will degrade in the body without releasing harmful byproducts.

Declaration of Competing Interest

The authors declare that they have no known competing financial interests or personal relationships that could have appeared to influence the work reported in this paper.

Data availability

Data will be made available on request.

Acknowledgments

The authors gratefully acknowledge the funding from the Swiss National Science Foundation (SNSF, grant N°200021_179064). The authors wish to thank Morgan Monroe and Dr. Jaemin Kim for their advice and suggestions, and ArjoWiggins Creative Papers for providing the paper samples.

Appendix A. Supplementary data

Supplementary data to this article can be found online at https://doi.org/10.1016/j.mne.2023.100218.

References

[1] M.M. Aung, Y.S. Chang, Temperature management for the quality assurance of a perishable food supply chain, Food Control 40 (2014) 198–207, https://doi.org/10.1016/j.foodcont.2013.11.016.
[2] T. Wu, J.-M. Redoute, M.R. Yuce, A wireless implantable sensor design with subcutaneous energy harvesting for long-term IoT healthcare applications, IEEE Access 6 (2018) 35801–35808, https://doi.org/10.1109/ACCESS.2018.2851940.
[3] H. Yin, Y. Cao, B. Marelli, X. Zeng, A.J. Mason, C. Cao, Soil sensors and plant wearables for smart and precision agriculture, Adv. Mater. 33 (2021) 2007764, https://doi.org/10.1002/adma.202007764.
[4] A.V. Quintero, F. Molina-Lopez, E.C.P. Smits, E. Danesh, J. van den Brand, K. Persaud, et al., Smart RFID label with a printed multisensor platform for environmental monitoring, Flex. Print. Electron. 1 (2016), 025003, https://doi.org/10.1088/2058-8585/1/2/025003.
[5] H.F. Arata, P. Löw, K. Ishizuka, C. Bergaud, B. Kim, H. Noji, et al., Temperature distribution measurement on microfabricated thermodevice for single biomolecular observation using fluorescent dye, Sensors Actuators B Chem. 117 (2006) 339–345, https://doi.org/10.1016/j.snb.2005.11.017.
[6] G.-S. Chung, J.-M. Jeong, Fabrication of micro heaters on polycrystalline 3C-SiC suspended membranes for gas sensors and their characteristics, Microelectron. Eng. 87 (2010) 2348–2352, https://doi.org/10.1016/j.mee.2010.04.005.
[7] S. Ali, A. Hassan, J. Bae, C.H. Lee, J. Kim, All-printed differential temperature sensor for the compensation of bending effects, Langmuir 32 (2016) 11432–11439, https://doi.org/10.1021/acs.langmuir.6b02885.
[8] A. Shuaibu Hassan, V. Juliet, Joshua Amrith Raj, C., MEMS based humidity sensor with integration of temperature sensor, Mater. Today Proc. 5 (2018) 10728–10737, https://doi.org/10.1016/j.matpr.2017.12.356.
[9] D.-C. Tranca, D. Rosner, R. Tataroiu, S.C. Stegaru, A. Surpateanu, M. Peisic, Precision and linearity of analog temperature sensors for industrial IoT devices, in: 2018 17th RoEduNet Conference: Networking in Education and Research (RoEduNet), Cluj-Napoca, IEEE, 2018, pp. 1–6, https://doi.org/10.1109/ROEDUNET.2018.8514122.
[10] N. Miyakawa, W. Legner, T. Ziemann, D. Telitschkin, H.-J. Fecht, A. Friedberger, MEMS-based microthruster with integrated platinum thin film resistance temperature detector (RTD), heater meander and thermal insulation for operation up to 1,000°C, Microsyst. Technol. 18 (2012) 1077–1087, https://doi.org/10.1007/s00542-012-1441-0.
[11] S.B.N. Gourikutty, D. Choong, R. Lim, M.R.N.B. Damalerio, J. Oh, Y. Kim, et al., Temperature detection system for Renal Denervation Catheter application, in: 2020 IEEE 22nd Electronics Packaging Technology Conference (EPTC), Singapore, IEEE, Singapore, 2020, pp. 198–202, https://doi.org/10.1109/EPTC50525.2020.9315073.
[12] N.P. Salowitz, Z. Guo, S.-J. Kim, Y.-H. Li, G. Lanzara, F.-K. Chang, Microfabricated expandable sensor networks for intelligent sensing materials, IEEE Sensors J. 14 (2014) 2138–2144, https://doi.org/10.1109/JSEN.2013.2297699.
[13] M.J. Tan, C. Owh, P.L. Chee, A.K.K. Kyaw, D. Kai, X.J. Loh, Biodegradable electronics: cornerstone for sustainable electronics and transient applications, J. Mater. Chem. C 4 (2016) 5531–5558, https://doi.org/10.1039/C6TC00678G.
[14] X. Yu, W. Shou, B.K. Mahajan, X. Huang, H. Pan, Materials, processes, and facile manufacturing for bioresorbable electronics: a review, Adv. Mater. 30 (2018) 1707624, https://doi.org/10.1002/adma.201707624.
[15] K.K. Fu, Z. Wang, J. Dai, M. Carter, L. Hu, Transient electronics: materials and devices, Chem. Mater. 28 (2016) 3527–3539, https://doi.org/10.1021/acs.chemmater.5b04931.
[16] W.B. Han, J.H. Lee, J. Shin, S. Hwang, Advanced materials and systems for biodegradable, transient electronics, Adv. Mater. 32 (2020) 2002211, https://doi.org/10.1002/adma.202002211.
[17] S.-W. Hwang, H. Tao, D.-H. Kim, H. Cheng, J.-K. Song, E. Rill, et al., A physically transient form of silicon electronics, Science 337 (2012) 1640–1644, https://doi.org/10.1126/science.1226325.
[18] C. Dagdeviren, S.-W. Hwang, Y. Su, S. Kim, H. Cheng, O. Gur, et al., Transient, biocompatible electronics and energy harvesters based on ZnO, Small 9 (2013) 3398–3404, https://doi.org/10.1002/smll.201300146.
[19] G.A. Salvatore, J. Sülzle, F. Dalla Valle, G. Cantarella, F. Robotti, P. Jokic, et al., Biodegradable and highly deformable temperature sensors for the internet of things, Adv. Funct. Mater. 27 (2017) 1702390, https://doi.org/10.1002/adfm.201702390.
[20] S.-K. Kang, R.K.J. Murphy, S.-W. Hwang, S.M. Lee, D.V. Harburg, N.A. Krueger, et al., Bioresorbable silicon electronic sensors for the brain, Nature 530 (2016) 71–76, https://doi.org/10.1038/nature16492.
[21] Q. Huang, Y. Zhu, Printing conductive nanomaterials for flexible and stretchable electronics: a review of materials, processes, and applications, Adv. Mater. Technol. 4 (2019) 1800546, https://doi.org/10.1002/admt.201800546.
[22] A. Falco, P.S. Sackenheim, F.J. Romero, M. Becherer, P. Lugli, J.F. Salmerón, et al., Fabrication of low cost and low impact RH and temperature sensors for the internet of environmental-friendly things, Mater. Sci. Eng. B 267 (2021), 115081, https://doi.org/10.1016/j.mseb.2021.115081.
[23] C. Bali, A. Brandlmaier, A. Ganster, O. Raab, J. Zapf, A. Hübler, Fully inkjet-printed flexible Temperature sensors based on carbon and PEDOT:PSS1, Mater. Today Proc. 3 (2016) 739–745, https://doi.org/10.1016/j.matpr.2016.02.005.
[24] X. Aeby, J. Bourely, A. Poulin, G. Siqueira, G. Nyström, D. Briand, Printed humidity sensors from renewable and biodegradable materials, Adv. Mater. Technol. (2022) 2201302, https://doi.org/10.1002/admt.202201302.
[25] B. Arman Kuzubasoglu, Bahadir S. Kursun, Flexible temperature sensors: a review, Sensors Actuators A Phys. 315 (2020), 112282, https://doi.org/10.1016/j.sna.2020.112282.
[26] Y.K. Lee, J. Kim, Y. Kim, J.W. Kwak, Y. Yoon, J.A. Rogers, Room temperature electrochemical sintering of Zn microparticles and its use in printable conducting inks for bioresorbable electronics, Adv. Mater. 29 (2017) 1702665, https://doi.org/10.1002/adma.201702665.
[27] S. Feng, Z. Tian, J. Wang, S. Cao, D. Kong, Laser sintering of Zn microparticles and its application in printable biodegradable electronics, Adv. Electron. Mater. 5 (2019) 1800693, https://doi.org/10.1002/aelm.201800693.
[28] B.K. Mahajan, B. Ludwig, W. Shou, X. Yu, E. Fregene, H. Xu, et al., Aerosol printing and photonic sintering of bioresorbable zinc nanoparticle ink for transient electronics manufacturing, SCIENCE CHINA Inf. Sci. 61 (2018), 060412, https://doi.org/10.1007/s11432-018-9366-5.
[29] J. Li, H. Xu, Z. Zhang, Y. Hao, H. Wang, X. Huang, Anhydride-assisted spontaneous room Temperature sintering of printed Bioresorbable electronics, Adv. Funct. Mater. 30 (2020) 1905024, https://doi.org/10.1002/adfm.201905024.
[30] D. Tobjörk, R. Österbacka, Paper electronics, Adv. Mater. 23 (2011) 1935–1961, https://doi.org/10.1002/adma.201004692.
[31] J.V.L. Alvarez, M.A. Larrucea, P.A. Bermúdez, B.L. Chicote, Biodegradation of paper waste under controlled composting conditions, Waste Manag. 29 (2009) 1514–1519, https://doi.org/10.1016/j.wasman.2008.11.025.
[32] Z. Fang, H. Zhang, S. Qiu, Y. Kuang, J. Zhou, Y. Lan, et al., Versatile wood cellulose for biodegradable electronics, Adv. Mater. Technol. 6 (2021) 2000928, https://doi.org/10.1002/admt.202000928.
[33] W. Li, Q. Liu, Y. Zhang, C. Li, Z. He, W.C.H. Choy, et al., Biodegradable materials and green processing for green electronics, Adv. Mater. 32 (2020) 2001591, https://doi.org/10.1002/adma.202001591.
[34] Y. Sui, M. Atreya, S. Dahal, A. Gopalakrishnan, R. Khosla, G.L. Whiting, Controlled biodegradation of an additively fabricated capacitive soil moisture sensor, ACS Sustain. Chem. Eng. 9 (2021) 2486–2495, https://doi.org/10.1021/acssuschemeng.0c07615.
[35] L. Yin, H. Cheng, S. Mao, R. Haasch, Y. Liu, X. Xie, et al., Dissolvable metals for transient electronics, Adv. Funct. Mater. 24 (2014) 645–658, https://doi.org/10.1002/adfm.201301847.
[36] H.-J. Hwang, K.-H. Oh, H.-S. Kim, All-photonic drying and sintering process via flash white light combined with deep-UV and near-infrared irradiation for highly conductive copper nano-ink, Sci. Rep. 6 (2016) 19696, https://doi.org/10.1038/srep19696.
[37] J. Perelaer, R. Abbel, S. Wünscher, R. Jani, T. van Lammeren, U.S. Schubert, Roll-to-roll compatible sintering of inkjet printed features by photonic and microwave exposure: from non-conductive ink to 40% bulk silver conductivity in less than 15 seconds, Adv. Mater. 24 (2012) 2620–2625, https://doi.org/10.1002/adma.201104417.
[38] Y.-R. Jang, S.-J. Joo, J.-H. Chu, H.-J. Uhm, J.-W. Park, C.-H. Ryu, et al., A review on intense pulsed light sintering technologies for conductive electrodes in printed electronics, Int. J. Precis. Eng. Manuf. Green Tech. 8 (2021) 327–363, https://doi.org/10.1007/s40684-020-00193-8.

[39] M. Atreya, G. Marinick, C. Baumbauer, K.V. Dikshit, S. Liu, C. Bellerjeau, et al., Wax blends as tunable Encapsulants for soil-degradable electronics, ACS Appl. Electron. Mater. 4 (2022) 4912–4920, https://doi.org/10.1021/acsaelm.2c00833.
[40] N. Fumeaux, D. Briand, Zinc hybrid sintering for printed transient sensors and wireless electronics. npj Flex, Electron 7 (2023) 14, https://doi.org/10.1038/s41528-023-00249-0.
[41] V.O. Nwoko, H.H. Uhlig, Logarithmic oxidation kinetics of zinc, J. Electrochem. Soc. 112 (1965) 1181, https://doi.org/10.1149/1.2423394.
[42] A.S.A. Chinelatto, A.L. Chinelatto, C.L. Ojaimi, J.A. Ferreira, E.M. Pallone, Effect of sintering curves on the microstructure of alumina–zirconia nanocomposites, Ceram. Int. 40 (2014) 14669–14676, https://doi.org/10.1016/j.ceramint.2014.06.055.
[43] V.M. Bogatyrev, N.V. Borisenko, V.A. Pokrovskii, Thermal Degradation of Polyvinylpyrrolidone on the Surface of Pyrogenic Silica 74, 2001, p. 6.
[44] Y. Borodko, H.S. Lee, S.H. Joo, Y. Zhang, G. Somorjai, Spectroscopic study of the thermal degradation of PVP-capped Rh and Pt nanoparticles in H_2 and O_2 environments, J. Phys. Chem. C 114 (2010) 1117–1126, https://doi.org/10.1021/jp909008z.
[45] R.B. Belser, W.H. Hicklin, Temperature coefficients of resistance of metallic films in the Temperature range 25° to 600°C, J. Appl. Phys. 30 (1959) 313–322, https://doi.org/10.1063/1.1735158.
[46] K.N. Zhu, Q. Ruan, A. Godfrey, The kinetics of grain growth in near-micrometre grain size copper produced by spark plasma sintering, IOP Conf. Ser. Mater. Sci. Eng. 89 (2015), 012060, https://doi.org/10.1088/1757-899X/89/1/012060.
[47] A. Singh, Grain-size dependence of temperature coefficient of resistance of polycrystalline metal films, Proc. IEEE 61 (1973) 1653–1654, https://doi.org/10.1109/PROC.1973.9345.
[48] S.V. Dukarov, S.I. Petrushenko, V.N. Sukhov, Inner size effect of temperature coefficient of resistance in Cu, Ag, V and Mo films, Vacuum 202 (2022), 111148, https://doi.org/10.1016/j.vacuum.2022.111148.
[49] W.B. Pietenpol, H.A. Miley, Electrical resistivities and temperature coefficients of lead, tin, zinc and bismuth in the solid and liquid states, Phys. Rev. 34 (1929) 1588–1600, https://doi.org/10.1103/PhysRev.34.1588.
[50] M.E. Hossain, M.I. Khan, C. Ketata, M.R. Islam, Comparative pathway analysis of paraffin and beeswax for industrial applications, J. Charact. Dev. Novel Mater. 13 (2023).
[51] Y. Zhang, J. Bi, S. Wang, Q. Cao, Y. Li, J. Zhou, et al., Functional food packaging for reducing residual liquid food: Thermo-resistant edible super-hydrophobic coating from coffee and beeswax, J. Colloid Interface Sci. 533 (2019) 742–749, https://doi.org/10.1016/j.jcis.2018.09.011.
[52] T.A.A. Nasrin, M.A. Rahman, M.S. Arfin, M.N. Islam, M.A. Ullah, Effect of novel coconut oil and beeswax edible coating on postharvest quality of lemon at ambient storage, J. Agric. Food Res. 2 (2020), 100019, https://doi.org/10.1016/j.jafr.2019.100019.
[53] F. Yilmaz, E. Dagdemir, The effects of beeswax coating on quality of Kashar cheese during ripening, Int. J. Food Sci. Technol. 47 (2012) 2582–2589, https://doi.org/10.1111/j.1365-2621.2012.03137.x.